Materials Research Proceedings 64 (2026) 291-298 https://doi.org/10.21741/9781644904091-36

High Performance 100 kW Axial Flux PMSM: Validation of the 9S/8P Configuration for Advanced Electric Drive Systems

Siti Nabilah ABDULLAH[1,a], Mohd Saufi AHMAD[1,b], Choo Jun TAN[2,c], Dahaman ISHAK[3,d], Qian Yee ANG[4,e], Chung Peng LIEW[5,f], Tow Leong TIANG[1,g*]

[1]Faculty of Electrical Engineering & Technology, Universiti Malaysia Perlis, Malaysia

[2]Faculty of Computing and Information Technology, Tunku Abdul Rahman University of Management and Technology, Kuala Lumpur University of Science and Technology, Malaysia

[3]Electrical Engineering Department, Prince Mohammad Bin Fahd University, Saudi Arabia

[4]Faculty of Chemical Engineering & Technology, Universiti Malaysia Perlis, Malaysia

[5]Low Carbon Lab, Malaysia

[a]sitinabilahh.abd@gmail.com, [b]saufiahmad@unimap.edu.my, [c]tancj@tarc.edu.my, [d]dbinishak@pmu.edu.sa, [e]qyang@unimap.edu.my, [f]liew.chunpeng@gmail.com, [g]towleong@unimap.edu.my

Keywords: Axial Flux, Permanent Magnet Synchronous Machine, Finite Element, Single Stator Double Rotor, Fractional Slot

Abstract. The research presents an intensive electromagnetic evaluation of a single stator double rotor (SSDR) axial flux permanent magnet (AFPM) machine, directly addressing the need for high power density solutions. The study investigates the 9s/8p fractional slot concentrated winding configuration, proving the viability of this SSDR unique topology. An advanced 3D Finite Element Analysis (FEA) technique models the machine and verifies performance under both open circuit and on load operation. The three main key findings are validating the high winding factor utilization, ensuring the SSDR configuration is effective to manage high current densities for steady state operation, and demonstrating a minimal torque fluctuation over one cycle. Thus, this analysis conclusively proves that the design of the SSDR machine has robust electromagnetic integrity and high reliability. Hence, the combination of 9s/8p of the AFPM machine is one of the prime candidates for next generation electric drive systems.

Introduction

The global shift toward sustainable energy systems necessitates developing highly efficient, power dense electrical machines [1]. Modern applications, such as direct drive wind turbines and in-wheel electric vehicle motors, demand compact designs with superior electromagnetic performance [2]. Due to the disc-shaped structure, axial flux permanent magnet (AFPM) machines have become a leading candidate. The disc-shaped configuration will naturally provide high power-to-weight and high torque-to-volume ratios [3].

To minimize pulsating forces and balance the winding factors, traditional PM machines frequently utilize a slot/pole combination such as 8s/12p [4]. Fractional slot concentrated windings (FSCW) have been favored recently because short end windings increase the fill factor and reduce copper losses of the machine [6]. However, a massive SSDR topology utilizing 9s/8p remains understudied in depth within current literature [7]. This particular SSDR configuration recently garnered attention, specifically for applications requiring high flux linkage characteristics [7]. Traditional overlapping winding in PM machines is what most early work concentrated on, verifying performance metrics and fundamental sizing [8]. Still, a critical knowledge gap

Content from this work may be used under the terms of the Creative Commons Attribution 3.0 license. Any further distribution of this work must maintain attribution to the author(s) and the title of the work, journal citation and DOI. Published under license by Materials Research Forum LLC.

Materials Research Proceedings 64 (2026) 291-298 https://doi.org/10.21741/9781644904091-36

concerning the performance boundaries of modern FSCW concepts has developed [9]. A detailed electromagnetic analysis of the slot/pole combination is needed to define the power density and the full operational envelope [10]. Also, prior work often omits comprehensive transient analysis, particularly the combined electromagnetic effects of full current loading on voltage and torque stability [11]. Therefore, this made the field data regarding the critical operating regime insufficient. This paper addresses the research gap regarding the lack of comprehensive electromagnetic performance and torque data for the 9s/8p SSDR AFPM machine by presenting a complete electromagnetic evaluation. Crucially, this paper focuses exclusively on the electromagnetic domain; it excludes necessary thermal analysis, demagnetization risk evaluation, and mechanical stress analysis crucial for validating the machine's long term integrity at 100kW.

This paper addresses the identified research gap by presenting a design and performance analysis of a 9s/8p SSDR AFPM machine, aimed at advanced electric transport applications. A 9s/8p detailed modeling and verification of the electromagnetic characteristics results verified using 3D finite element analysis (FEA) is the key contribution.

Machine Design and Analytical Modeling

An AFPM machine topology consists of a few constructions. The three main structures have been listed in Figure 1. The basic construction of AFPM design is single stator single rotor (SSSR), employing one magnetic interaction surface. Next is a single stator double rotor (SSDR), in which the structure sandwiches the stator between two rotors. Last but not least is the double stator single rotor (DSSR) type, in which the rotor is located centrally between two stators. Each arrangement offers unique tradeoffs concerning mechanical rigidity and output power density, guiding application-specific selection.

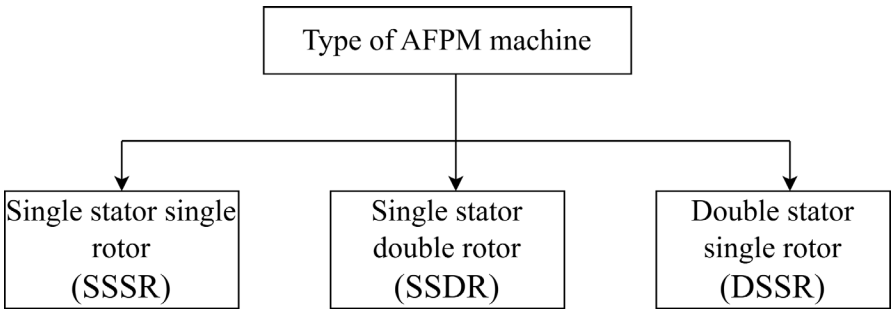


Figure 1: Three generic configurations of the AFPM machine

This research employs the SSDR structure, where the configurations consist of a single stator sandwiched between two rotors [12]. A full illustration of the 9s/8p SSDR AFPM machine is displayed in Figure 1. The machine configuration uses a non-overlapping winding with a Torus NN configuration. Also, Ansys Electronics Desktop is used to do the electromagnetic simulation. The selection of 9s/8p pairs is because this combination gives the highest fundamental winding factor at the slot-per-pole-per-phase ratio. Moreover, the least common multiple (LCM) of 72 effectively minimizes inherent torque ripple, ensuring the machine achieves high performance. The parameters of the machine are displayed in Table 1.

Materials Research Proceedings 64 (2026) 291-298 https://doi.org/10.21741/9781644904091-36

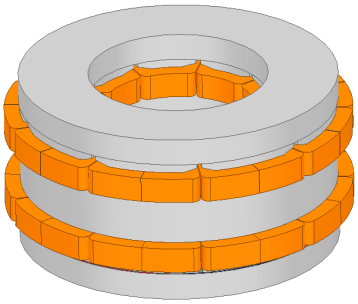


Figure 2: 9s/8p SSDR configuration

Table 1: Geometry of 9s/8p AFPM machine

Parameter	Value	Parameter	Value
Output Power, P_{out}	100 kW	Pole number, N_p	8
Frequency, f	100 Hz	Slot number, N_s	9
Air gap length, l_g	1.00 mm	Turns per phase, N_{tph}	96
Current density, J	5×10^6 A/m^2	Stator length, L_s	202.00 mm
Phase RMS Current, I_{rms}	74.00 A	Total axial length, L_{ax}	296.05 mm
Remanence, B_r	1.2 T	Magnet material	Arnold_N35

A sizing equation is introduced to establish the dimensions of the AFPM machine, incorporating the determination of the number of slots, poles, operating frequency, and air gap length. The output power of the electrical machine, denoted as P_{out}, can be calculated as follows [13]

$$P_{out} = \eta m K_p E_{pk} I_{pk} \tag{1}$$

where η quantifies efficiency, m denotes the phase number, K_p shows the power waveform factor, and E_{pk} and I_{pk} denote the peak voltage and current. The generalized sizing equation is as follows [14]:

$$P_{out} = \left(\frac{1}{1+K_\phi}\right)\left(\frac{m}{m_1}\right)\left(\frac{\pi}{2}\right) K_e K_i K_p \eta B_g A \left(\frac{f}{p}\right)\left(1-\lambda^2\right) D_O^2 \tag{2}$$

where $m1$ is the number of stator phases, K_ϕ is the ratio of rotor to stator electrical loading, the electromagnetic force (EMF) factor, K_e, incorporates the effects of the winding distribution and the pole enclosure within the air gap, K_i is the current waveform factor, A represents the stator electrical loading, B_g is the average flux density in the air gap, the electrical frequency f, and the number of pole pairs p. The geometric proportions of the machine are defined by the diameter ratio $\lambda = D_i/D_o$, where D_o *and* D_i are the outer and inner diameters, respectively. Expressions determine the peak voltage, E_{pk} [15]

$$E_{pk} = K_e N_{tph} B_g \left(f / p\right)\left(1-\lambda^2\right) D_o^2 \tag{3}$$

where N_{tph}, the number of turns per phase. The equation for the total axial length, L_{ax}, provides an initial estimate for the structure:

Materials Research Proceedings 64 (2026) 291-298 https://doi.org/10.21741/9781644904091-36

$$L_{ax} = 2(L_{cr} + L_{pm}) + 2l_g + L_{cs} + 2d_{ss} \tag{4}$$

where L_{cr} defines the length of the rotor core, L_{pm} represents the depth of PM, l_g specifies the air gap length, L_{cs} gives the length of the stator core, and d_{ss} provides the stator slot length. The B_g formula for the air gap flux density follows immediately:

$$B_g = B_{rm} / \left[1 + \left(\mu_r l_g / L_{pm}\right)\right] \tag{5}$$

where μ_r is relative permeability and B_{rm} is magnetic remanence.

Simulation Analysis

A flux density waveform during open circuit condition is shown in Figure 3. The peak of the flux density waveform reaches approximately 0.9T in the magnetic regions. The inclusion of this waveform over 180 degrees produces an average air gap flux density of roughly 0.75 T, validating high magnetic utilization for energy conversion. This high magnitude verifies the high magnetic loading necessary for the 100 kW power requirement. Critically, the measurement exposed pronounced high order spatial harmonics, manifesting as sharp fluctuations along the pole faces. Hence, harmonics are caused by slot openings.

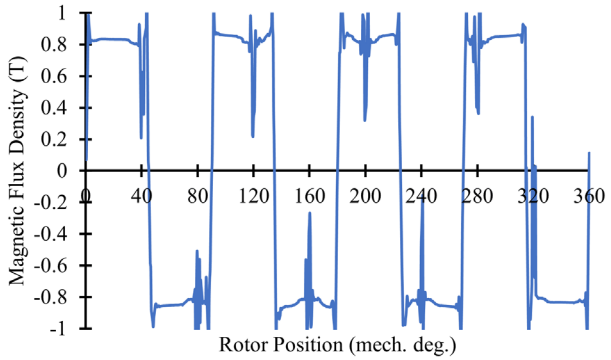


Figure 3: Flux density waveform during open circuit condition

Moving on, Figure 4 displays the magnetic flux density distribution of the 9s/8p SSDR AFPM machine during open circuit condition. Flow lines successfully illustrate the magnetic circuit, validating flux travels axially from the surface inserts magnets on both rotors, and successfully links through the central stator teeth. The color indicator indicates that a high concentration area is up to 1.74 T, concentrated mainly within the stator yoke and teeth. Therefore, this validates high quality electrical steel successfully channels the dense magnetic energy necessary for maximum torque production. To conclude, the design effectively manages high saturation levels, allowing the machine to achieve the required output capacity validated in this analysis.

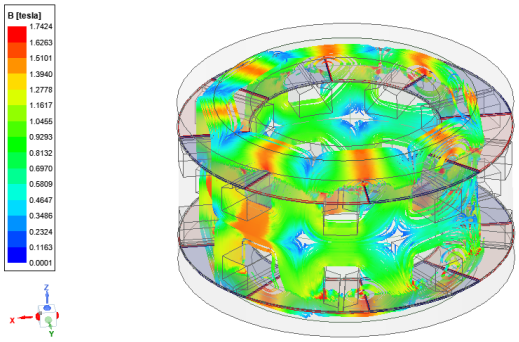


Figure 4: Magnetic flux density distribution of the 9s/8p SSDR AFPM machine during open circuit condition

Next, illustrated in Figure 5, is the induced voltage during the open circuit condition. The analytical prediction during open circuit condition is confirmed, with a RMS phase voltage consistently peaking close to 500V. The waveform shown is nearly sinusoidal, fundamental to the 9s/8p combination. The balanced three phase waveform verifies that the machine generates a rotating magnetic field. Moreover, the capability of the machine in delivering the output power is confirmed at the rated frequency during a high voltage magnitude.

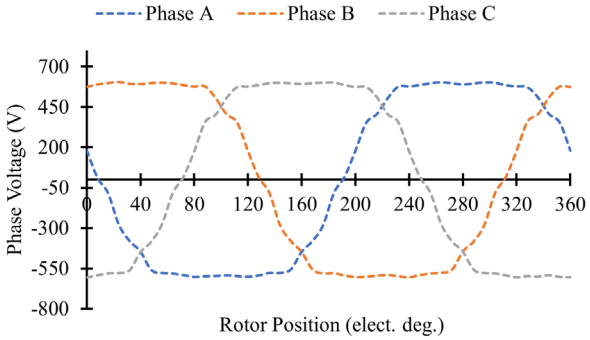


Figure 5: Induced voltage during the open circuit condition

Following next, Figure 6 depicts a total harmonic distortion of voltage during an open circuit condition. The third harmonic during analysis shows a strong presence, which prevails in the spectrum. Meanwhile, the rest of the harmonics, such as the fifth and higher-order components, present very low magnitudes. In return, the overall total harmonic distortion (THD) is at a low, acceptable value. Therefore, the harmonic losses of the machine are reduced and capable of delivering a high quality sinusoidal voltage, guaranteeing seamless integration with the high power electronic drive.

Subsequently, the induced voltage during the on load condition is presented in Figure 7. The waveform of the voltage sustains a symmetrical balance. The peak of the phase voltage is nearly 900V, proving the ability of the machine to produce the 100kW output power. Also, a robust electromagnetic performance during on load is established due to the voltage results that effectively drive the PM motor. Additionally, the robust magnetic coupling between the PM and the fractional slot winding is confirmed. Overall, the design of the SSDR machine intrinsically has the capacity to maintain electrical loading.

Materials Research Proceedings 64 (2026) 291-298 https://doi.org/10.21741/9781644904091-36

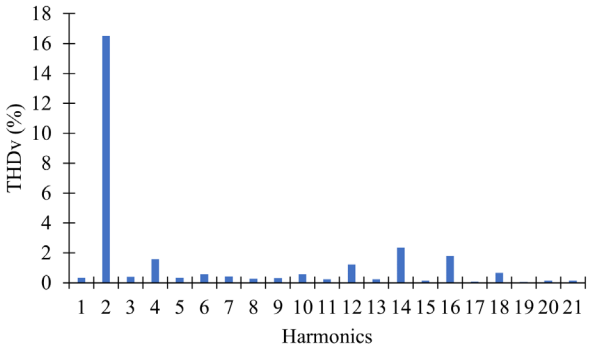


Figure 6: THDv during an open circuit condition

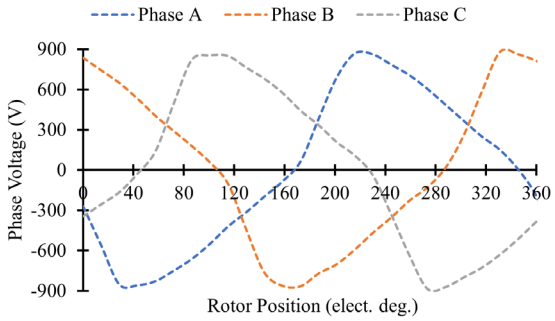


Figure 7: Induced voltage during the on load condition

As well as the waveforms of the induced phase voltage and the excitation stator current during on load condition are displayed in Figure 8. The peak of the voltage waveform is nearly 900V, verifying the electrical parameters performance, confirming that the design achieves the 100kW output power. A maximum of 100A amplitude is demonstrated in a nearly sinusoidal waveform, which is captured in the current waveform. To wrap up, the machine sustains the rated operating condition for maximum power utilization, validating the output potential.

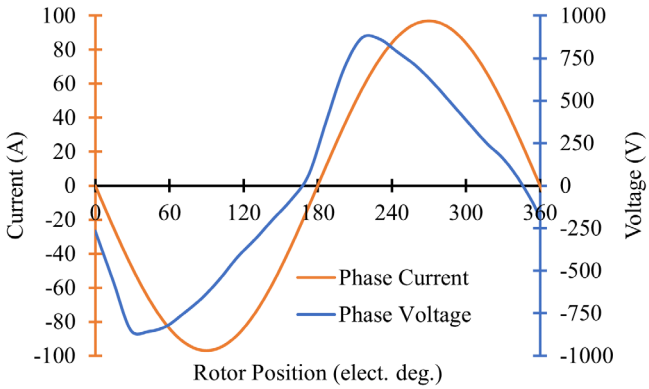


Figure 8: Induced phase voltage versus excitation stator current during on load condition

Lastly, Figure 9 shows the output power versus electromagnetic torque during on load condition. During the electrical rotation, the output power remains closely confined around 100 kW. At the same time, the torque that the validating machine produces is the required 637 Nm. Hence, the machine achieves robust mechanical stability for high power density drive applications.

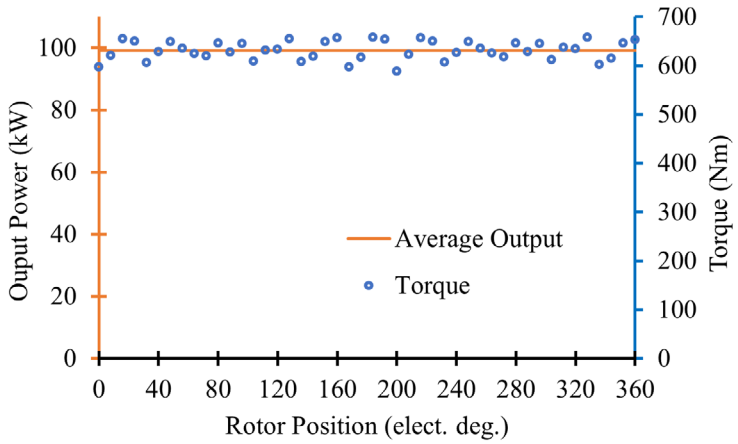


Figure 9: Output power and electromagnetic torque waveform during on load condition

Summary

The analysis of the 9s/8p SSDR AFPM design validated that the design reaches exceptional operational integrity. Magnetic vector analysis proves the SSDR configuration effectively channels the magnetic field along the axial path, producing a peak flux density of almost 0.9 T. This established strong field creates a clean, quasi-trapezoidal flux waveform, confirming high magnetic utilization. Field visualizations further confirm that the high quality electrical steel successfully channels dense magnetic flux through the central stator yoke, managing saturation levels. Electrically, the induced voltage waveform exhibits symmetrical three phase characteristics under no load, confirming 500 V_{rms} output. Under on load condition, the voltage profile remains robust, peaking near 900 V and confirming the machine sustains the entire 100 kW requirement. Furthermore, the harmonious interaction between the voltage waveform and the applied current successfully drives the full 637 Nm of rated torque, validating stable electromagnetic performance under heavy demand and confirming high magnetic coupling for sustainable full power utilization.

Aknowledgement

The authors would like to acknowledge the support from the Ministry of Higher Education (MoHE) Malaysia through the Fundamental Research Grant Scheme (FRGS) under a grant number of FRGS/1/2023/TK02/UNIMAP/02/5.

References

[1] L. Shao, R. Navaratne, M. Popescu, and G. Liu, "Design and Construction of Axial-Flux Permanent Magnet Motors for Electric Propulsion Applications-A Review," IEEE Access. 2021. https://doi.org/10.1109/ACCESS.2021.3131000

[2] J. Zhao, X. Liu, S. Wang, and L. Zheng, "Review of Design and Control Optimization of Axial Flux PMSM in Renewable-energy Applications," Chinese Journal of Mechanical Engineering (English Edition). 2023. https://doi.org/10.1186/s10033-023-00868-8

[3] Z. Hao, Y. Ma, P. Wang, G. Luo, and Y. Chen, "A Review of Axial-Flux Permanent-Magnet Motors: Topological Structures, Design, Optimization and Control Techniques," Machines. 2022. https://doi.org/10.3390/machines10121178

[4] S. W. Song, S. H. Lee, and W. H. Kim, "Design and Analysis of Consequent Pole Axial Flux Motors for Reduced Torque Ripple and Magnet Consumption," Processes, vol. 13, no. 7, pp. 1-15, 2025. https://doi.org/10.3390/pr13072139

[5] S. Ravindran, P. Koothu Kesavan, D. Banjerdpongchai, and P. Prem, "Modelling, implementation and analysis of double-side slotted axial flux PMGs suitable to small-scale wind energy conversion systems," Sci. Rep., vol. 15, no. 1, pp. 1-20, 2025. https://doi.org/10.1038/s41598-025-08716-6

[6] I. A. Rudden, G. J. Li, Z. Q. Zhu, A. Duke, and R. Clark, "Fractional-Slot Concentrated Windings for Offshore Wind Turbine Generators: Opportunities and Challenges," IEEE Access, vol. 12, no. September, pp. 158766-158787, 2024. https://doi.org/10.1109/ACCESS.2024.3486000

[7] S. Y. Kim, "A study on motor characteristics based on pole-slot combinations," AIP Adv., vol. 14, no. 1, pp. 10-15, 2024. https://doi.org/10.1063/9.0000647

[8] X. Sun, Z. Q. Zhu, S. Cai, L. Wang, F. R. Wei, and B. Shao, "Influence of Stator Slot and Rotor Pole Number Combination on Field Winding Induced Voltage Ripple in Hybrid Excitation Switched Flux Machine," IEEE Trans. Energy Convers., vol. 36, no. 2, pp. 1245-1261, 2021. https://doi.org/10.1109/TEC.2020.3035258

[9] A. M. EL-Refaie, "Fractional-slot concentrated-windings synchronous permanent magnet machines: Opportunities and challenges," IEEE Trans. Ind. Electron., vol. 57, no. 1, pp. 107-121, 2010. https://doi.org/10.1109/TIE.2009.2030211

[10] D. Quan et al., "The Design, Analysis, and Verification of an Axial Flux Permanent Magnet Motor with High Torque Density," Appl. Sci., vol. 15, no. 6, 2025. https://doi.org/10.3390/app15063327

[11] J. F. Zhao, X. Y. Liu, S. Wang, and L. X. Zheng, "Review of Design and Control Optimization of Axial Flux PMSM in Renewable-energy Applications," CHINESE J. Mech. Eng., vol. 36, no. 1, 2023. https://doi.org/10.1186/s10033-023-00868-8

[12] S. Sarıdağ and M. Eker, "Design of Double-Stator Axial Flux Permanent Magnet Synchronous Motor," J. New Results Eng. Nat. Sci., vol. 2024, no. 21, pp. 30-46, 2024.

[13] O. Shariati, A. Behnamfar, and B. Potter, "An Integrated Elitist Approach to the Design of Axial Flux Permanent Magnet Synchronous Wind Generators (AFPMWG)," Energies, 2022. https://doi.org/10.3390/en15093262

[14] S. Kahourzade, A. Mahmoudi, H. W. Ping, and M. N. Uddin, "A comprehensive review of axial-flux permanent-magnet machines," Canadian Journal of Electrical and Computer Engineering. 2014. https://doi.org/10.1109/CJECE.2014.2309322

[15] R. Pormoozeh-Noveiry and M. Niaboli-Guilani, "Optimizing the Efficiency of a Three Phase Axial Flux Synchronous Generator for Use in Direct-Drive Wind Turbines and Modeling by 3D Finite Element Method," in 2023 5th International Conference on Optimizing Electrical Energy Consumption, OEEC 2023, 2023. https://doi.org/10.1109/OEEC58272.2023.10135483